Politecnico di Torino

Porto Institutional Repository

[Article] Role of repulsive factors in vascularization dynamics

(Article begins on next page)
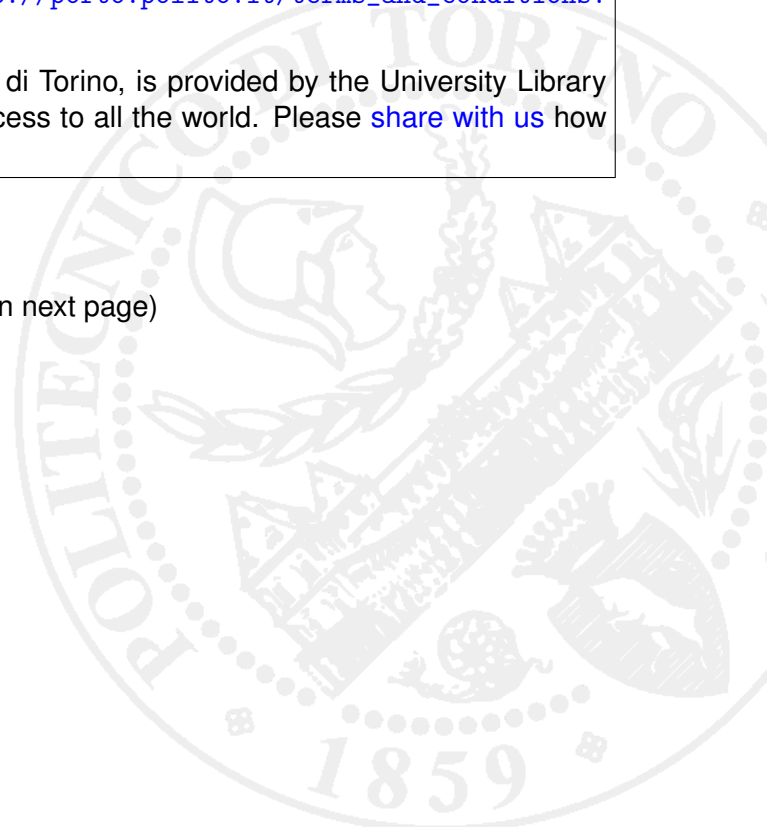
Role of repulsive factors in vascularization dynamics

S. Di Talia,[1,*] A. Gamba,[2,†] F. Lamberti,[3,‡] and G. Serini[4,§]

[1]*Laboratory of Mathematical Physics, The Rockefeller University, New York, New York 10021, USA*

[2]*Dipartimento di Matematica, Politecnico di Torino and INFN, unit of Torino, 10129 Torino, Italy*

[3]*Dipartimento di Automatica e Informatica, Politecnico di Torino, 10129 Torino, Italy*

[4]*Department of Oncological Sciences, University of Torino and Institute for Cancer Research and Treatment, 10060 Candiolo (TO), Italy*

Capillary networks are essential in vertebrates to supply tissues with nutrients. Experiments of *in vitro* capillary formation show that endothelial cells randomly spread on a gel matrix autonomously organize to form vascular networks with a characteristic length independent of the initial cell density. A mathematical model based on free cell migration and on cell cross-talk mediated by soluble chemical factors has been recently proposed and explains the main dynamical and geometrical properties of the networks. We extend this model introducing the action of repulsive factors and we show that their activity results in a larger degree of reorganization of cellular matter and in more robust control over the size of the growing vascular network.

PACS number(s): 87.18.Hf, 87.10.+e, 87.17.−d

I. INTRODUCTION

Biological systems are characterized by large numbers of functionally similar elements that interact selectively and nonlinearly to produce a complex behavior. These systems often show elaborate hierarchies of feedback regulation [1,2]. Feedback mechanisms are often based on both attractive and repulsive signaling molecules.

The need for repulsive factors in cellular aggregation processes has been known for a long time [3]. The presence of these factors along with attractive ones produces instabilities that drive the process of pattern formation with morphological characteristics determined by the rates of the chemical reactions and diffusion.

In vascularization dynamics, the role played by repulsive factors is a subtle one. Recent research has shown that repulsive factors are required to endow the biological system with the necessary degree of plasticity and robustness, allowing a graded control of cellular migration rate and redirectioning during migration [4].

Cellular aggregation is central in blood vessel formation, a process that has been thoroughly studied experimentally for its fundamental relevance in many physiological and pathological conditions [5]. Experimental assays of the process have been devised which allow a high degree of reproducibility and control of parameters. Biological insight obtained this way has led to the formulation of a concise mathematical model that explains the main dynamical and geometrical properties of experimental vascular network formation [6]. The good agreement of the model predictions with observations provides evidence that experimental capillary network formation (vasculogenesis) is driven by a cross-talk mechanism, where cells release and respond to chemoattractive soluble factors that stimulate motility [7]. Recent experiments in mice have confirmed the proposed autocrine cross-talk mechanism showing its essential role in *in vivo* angiogenesis [8]. Since chemoattractive factors have a finite lifetime, this introduces in the model a typical length scale and suggests that Nature realizes this way a control on the characteristic size of capillary networks. This is confirmed by the experimental observation that the characteristic length scale introduced with the initial conditions, which is a typical cell-cell distance and is a function of the initial cell density, is disrupted by a dynamical process that rearranges the structures on a constant length scale of the order of the diffusion range of the soluble factors. Further, independent confirmation is likely to come from experiments on mice [9] where deletion of growth factors with smaller diffusivities results in larger capillary network sizes. In particular, the experimental results of Ref. [9] are strikingly reminiscent of the model simulations of Ref. [7].

Let us notice here that the existence of a control mechanism on the size of capillary networks should come as no surprise, since intercapillary distances ranging between 50 and 300 μm are required for optimal metabolic exchange [10]. As a matter of fact, the capillary networks of the vertebrates are all characterized by these characteristic dimensions.

A natural extension of the model [6,7] consists of taking into account the action of soluble repulsive factors, which are known to play a biologically relevant role. Their inclusion in the dynamical scheme should allow us to test quantitatively current ideas about their role and action. In this paper, we study the effect of this extension through analytical arguments and computer simulations and find that the action of repulsive factors results in a larger degree of reorganization of cellular matter and in more robust control over the size of the growing vascular network.

The ability to reorganize vascular networks is of peculiar relevance in living beings, e.g., during embryonic growth [11] and in the healing of wounds [12]. Our numerical simu-

*Electronic address: stefano@orbis.rockefeller.edu

†Electronic address: andrea.gamba@polito.it

‡Electronic address: fabrizio.lamberti@polito.it

§Electronic address: guido.serini@ircc.it

lations show that starting from commonly realized experimental conditions where cells are initially randomly dispersed on a flat surface, the dynamical system generated by the diffusion of an attractive and a repulsive chemical factor allows for a larger degree of reorganization of cellular matter with respect to the situation where only an attractive factor is present. This is due to the "screening" effect realized by the repulsive factor in the cell proximity, which allows for a more even distribution of the attractive signal in space and a more efficient reorganization dynamics.

A second function performed by repulsive factors is to provide robustness and sharpness of the size control mechanism. We show that both properties are strictly related to the analytic properties of the integral kernel, which appears in the solution of the equation for the diffusion of chemical substances. This kernel can depress wavelengths that are, respectively, larger and smaller than the chemical range, acting as a band-pass filter in the spatial domain. Our analysis shows that in order to have a sharper and more robust control on the structure size, at least an attractive and a repulsive signal must be present. We expect that this prediction can be verified experimentally.

The paper is organized as follows. Section II summarizes some background knowledge on the biology of vascular network formation. In Sec. III, we introduce the model and study the analytical properties of the integral kernel that appears in the solution of the relevant diffusion equations. Section IV contains numerical results and analysis of the geometry of vascular structures. In Sec. V, we conclude discussing the possible relevance of our results for future studies. In the Appendix, we present the algorithm used for image analysis.

II. EXPERIMENTAL VASCULOGENESIS

Experiments of *in vitro* vascularization are an ideal test for theories of vascularization dynamics because the main parameters are under control: for instance, it is possible to perform experiments with a given cellular population, with the same values of physical parameters and with the same initial conditions, and one can track cell motion with great precision through noninvasive means such as videomicroscopy. Experiments can be repeated many times, so that statistical methods can be used to get quantitative information on the system.

In the experiments, endothelial cells are randomly dispersed on Matrigel, a surface which favors cell motility and has biochemical characteristics similar to living tissues, and observed while they autonomously organize to form a two-dimensional network and roll up to form vascular tubes [13,14] (Fig. 1). The whole process needs 12–14 h to complete. An accurate statistics of individual cell trajectories has been presented in Ref. [7], showing that in the early stages of network formation, cell motion has marked directional persistence, pointing toward zones of a higher concentrations of cells.

The capillarylike network is a collection of nodes connected by chords. The mean chord length has the approximately constant value $\ell_0 \simeq 200$ μm over a range of values of the density $\bar{n}$ extending from 100 to 250 cells/mm^2. Corre-

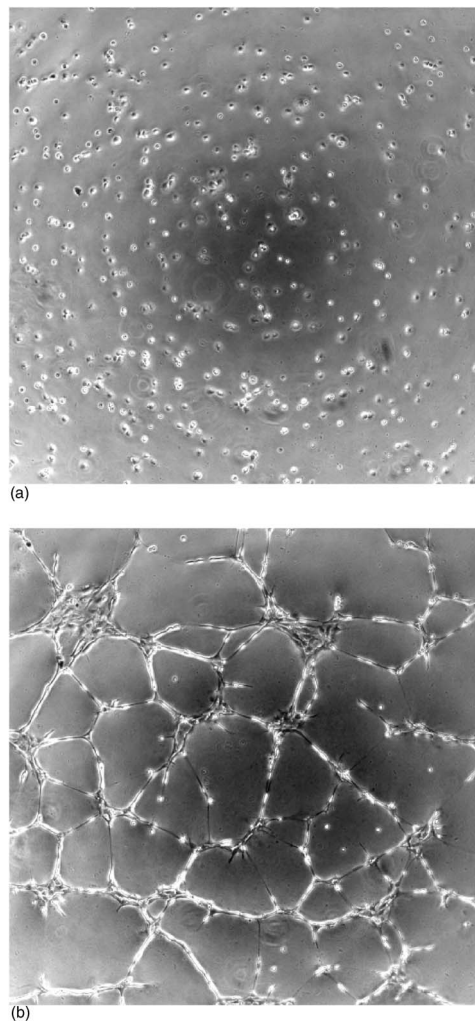FIG. 1. (a) Cells are randomly deposed at time $t=0$ on a Matrigel surface of size $L^2 = 4$ mm^2. (b) End point of autonomous cell aggregation in a capillary-like network, at time $t=9$ h.

spondingly, the mean chord thickness grows to accommodate an increasing number of cells. Eventually, one observes a continuous carpet of cells interspersed with holes [7]. By varying $\bar{n}$, one observes a percolative phase transition [6,15].

In Ref. [6], evidence has been provided that a control on the size of capillary networks is realized through the exchange among cells of attractive soluble factors. The model does not make any assumption on the nature of these factors. Our group [7] and others [8,16–19] have shown evidence that during vascular network formation, both *in vitro* and *in vivo* the autocrine attractive factors essential for pattern formation may be represented by the VEGF-A (vascular endothelial growth factor). VEGF-A has a finite average lifetime $\tau \simeq 1$ h, resulting in a finite interaction radius ($r_A \sim 200$ μm) which turns out to be of the order of the characteristic network size. However, the model proposed in Ref. [6] is simplified. Along with attractive factors, endothelial cells are known to secrete repulsive factors [4]. Attractive factors themselves exist in several isoforms [20], characterized by diffusivities that can vary by factors of order 1 [21]. Taking into account these finer effects could lead to a proper
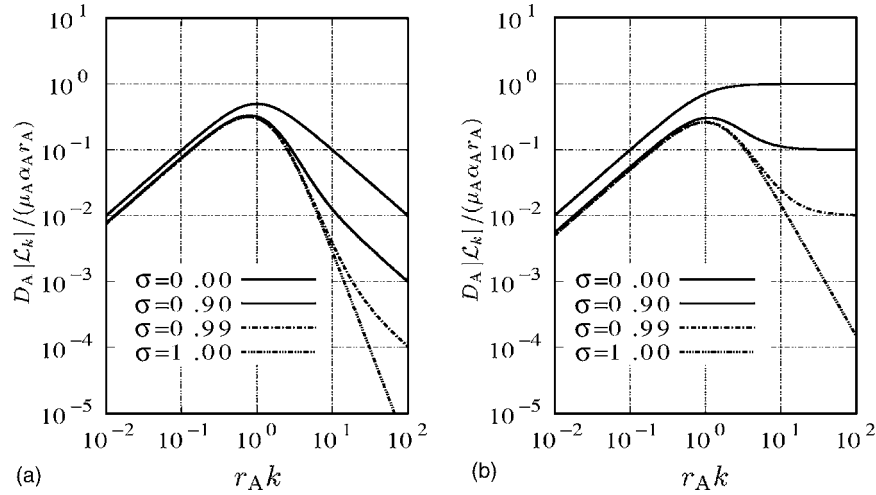
FIG. 2. Log-log graph of the module of the transfer function $\mathcal{L}_{\mathbf{k}}$ (Bode plot) for (a) diffusion in a two-dimensional environment and (b) in a three-dimensional one for various relative contributions of attractive and repulsive factors σ. For simplicity, we let $\mu_A \alpha_A / D_A = 1$ and choose r_A as length scale unit, while $r_R = r_A / 2$.

understanding of the experimental results of Ref. [9]. Furthermore, it is known that isoforms of VEGF-A act in a coordinated fashion to recruit and expand tumor vasculature [22].

III. THE MODEL

A. General framework

We propose here a generalization of the model of Ref. [6] that takes into account the existence of several types of soluble factors, characterized by different diffusivities and chemical actions (attractive or repulsive). The endothelial cell population is described by a continuous distribution of density n and Eulerian velocity $\mathbf{v}$, and we assume the presence of F families of soluble molecules, whose concentrations are denoted, respectively, by $c_1, \ldots, c_F$.

We shall study in more detail the two-field model where c_A and c_R represent, respectively, the concentrations of attracting and repulsive factors. For the sake of simplicity, we consider a linear response of cells to the concentration of soluble factors. The model presented in Ref. [6] is then generalized to the following equations:

$$\frac{\partial n}{\partial t} + \nabla \cdot (n\mathbf{v}) = 0, \tag{1a}$$

$$\frac{\partial \mathbf{v}}{\partial t} + \mathbf{v} \cdot \nabla \mathbf{v} = \nabla \sum_{k=1}^{F} \mu_k c_k - f(n)\mathbf{v}, \tag{1b}$$

$$\frac{\partial c_k}{\partial t} = D_k \nabla^2 c_k + \alpha_k n - \tau_k^{-1} c_k \quad (k = 1, \ldots, F), \tag{1c}$$

where D_k, α_k, τ_k $(k=1,\ldots,F)$ are, respectively, the diffusion coefficient, the rate of release, and the characteristic degradation time of the kth soluble factor, and μ_k, which is assumed to be positive for attractive factors and negative for repulsive factors, measures the strength of the cell response

to the concentration gradient ∇c_k. In the experiments, cells are initially randomly distributed on Matrigel. We therefore impose initial conditions in the form of a set of randomly distributed bell-shaped bumps of unitary volume having width of the order of the average cell radius, with null velocities.

Regularity of solutions and approach to a stationary state can be obtained by the addition on the right-hand side (r.h.s.) of Eq. (1b) of *ad hoc* phenomenological terms [6,15,23]. These terms are not really essential and just provide a clean way of mimicking the biological system by freezing the evolution when cells get close together. In this paper, we shall make use of a density-dependent linear friction term $-f(n)\mathbf{v}$, where $f(n)$ is zero for low densities and increases rapidly above a threshold of a few times the heights of the initial bumps [24]. The biological motivation for this term is that cells establishing reciprocal contacts are observed to progressively slow down migration, as if cell-cell contacts switched off migration in favor of the establishment of stronger binding to the gel matrix [7].

In the fast diffusion approximation, i.e., neglecting the time derivative on the left-hand side (l.h.s.) of Eq. (1c), it is possible to solve for c_k and to substitute in Eq. (1b), obtaining the simpler system

$$\frac{\partial n}{\partial t} + \nabla \cdot (n\mathbf{v}) = 0, \tag{2a}$$

$$\frac{\partial \mathbf{v}}{\partial t} + \mathbf{v} \cdot \nabla \mathbf{v} = \mathcal{L}n - f(n)\mathbf{v}, \tag{2b}$$

where $\mathcal{L} = \sum_{k=1}^{F} (\mu_k \alpha_k / D_k) \cdot \nabla (r_k^{-2} - \nabla^2)^{-1}$ and $r_k = \sqrt{D_k \tau_k}$ is the characteristic interaction range of the kth chemical factor [25].

The dynamical behavior of system (1) is as follows. Initially, nonzero velocities are built up by the chemoattractive term due to the presence of random inhomogeneities in the density distribution. Then, Burgers' dynamics amplifies the

inhomogeneities and forms a capillarylike network. Density inhomogeneities are translated in a landscape of concentration of soluble factors where details of scales $\leq r_k$ are averaged out. Particles move toward the crests of the landscape, which are separated by valleys of width $\sim r_k$. Burgers' dynamics sharpens the crests and empties the valleys in the concentration landscape, eventually producing a network structure characterized by a length scale of order r_k. This is a transient regime, chords are unstable, and eventually matter will collapse into the nodes. The introduction of a pressure, friction, or contact inhibition term on the r.h.s. of Eq. (1b) prevents matter collapse into the nodes and provides a clean way to mimic the biological system.

B. Reorganization and robust control

Let us study in more detail the two-field model, where c_A and c_R are, respectively, the concentrations of attractive and repulsive factor. In this case, the relevant parameters are the diffusive lengths r_A and r_R and the ratio $\sigma = |\mu_R| \alpha_R D_A / \mu_A \alpha_A D_R$ [26]. Repulsive factors are heavier molecules ($\sim 2 \times 10^5$ a.m.u.) than attractive factors ($\sim 3 \times 10^4$ a.m.u.) and have shorter diffusive length [4]: we therefore assume $r_A > r_R$. According to available data, the order of magnitude of the diffusion coefficient and the characteristic time of degradation of attractive chemical factors such as VEGF-A 165 are $D_A \sim 10^{-7}$ cm^2 s^{-1} and $\tau_A \sim 4000$ s, giving $r_A \sim 200$ μm [7,27]. Precise quantitative data are not available for repulsive factors.

Equation (1b) is a Burgers-like equation for $\mathbf{v}$ [28], coupled to the standard diffusion equations (1c). In the absence of any coupling with soluble mediators, Eqs. (1a) and (1b) are reminiscent of the adhesion model [29]. It is a well known characteristic of that model, investigated both analytically and numerically, that small inhomogeneities in the initial conditions are amplified by the dynamics and eventually lead to the formation of structures, which in two dimensions are strikingly similar to those of capillary networks [30]. The coupling with the two fields of soluble mediators introduces in the model two characteristic lengths r_A, r_R, which are likely to be observable in the geometry of the resulting network, according to the scheme outlined in Ref. [6]. The coupling is established (in the fast diffusion approximation) through the source term $\mathcal{L}n$, where the Fourier transform of $\mathcal{L}$ is

$$\mathcal{L}_{\mathbf{k}} = \left(i \frac{\mu_A \alpha_A}{D_A} \right) \left(\frac{\mathbf{k}}{r_A^{-2} + k^2} - \sigma \frac{\mathbf{k}}{r_R^{-2} + k^2} \right).$$

It is easily seen that the action of this operator has the effect of depressing the wavelengths of the density field which are larger or smaller than r_A. This means that $\mathcal{L}_{\mathbf{k}}$ acts as a bandpass filter in the spatial domain.

The Fourier transform $\mathcal{L}_{\mathbf{k}}$ can be seen as the transfer function for the nonlinear feedback loop realized by the system (2). The properties of $\mathcal{L}_{\mathbf{k}}$ at varying values of σ are conveniently summarized in a Bode magnitude plot [Fig. 2(a)], showing the asymptotic behavior of the filter for small and large wave numbers. For $\sigma = 0$ (no repulsive factor) and $k \gg r_A^{-1}$, $|\mathcal{L}_{\mathbf{k}}| \sim 1/k$. For $\sigma = 1$, one has a higher-order filter
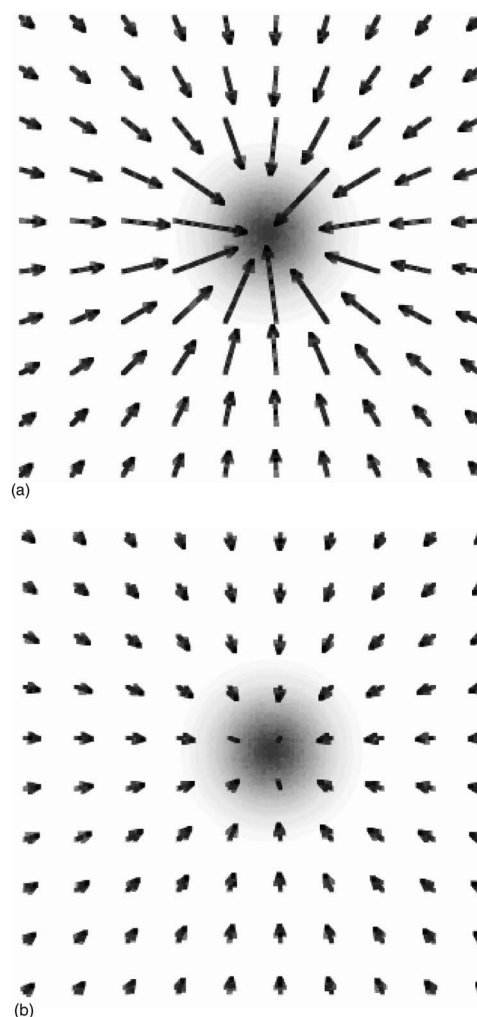

FIG. 3. Distribution of attractive and repulsive factors in the neighborhood of a bump of cellular matter, in the presence of a purely attractive factor c_A [panel (a)] and of both attractive and repulsive factors c_A and c_R [panel (b)]. (a) Distribution of c_A and graph of the gradient field ∇c_A. (b) Distribution of $c_A - c_R$ and graph of the gradient field $\nabla(c_A - c_R)$.

characterized by the asymptotic behavior $|\mathcal{L}_{\mathbf{k}}| \sim 1/k^3$, corresponding to a sharper bandwidth and a higher selectivity. For intermediate values $\sigma \lesssim 1$, one observes a crossover for $k \sim 1/\sqrt{1-\sigma}$ to the $\sigma = 0$ behavior.

The control properties of the transfer function $\mathcal{L}_{\mathbf{k}}$ influence the geometry of the network structures formed by the evolution of Eq. (1) from random initial conditions. Initially, cells are seeded in random positions. This introduces in the model the length scale $r_{\text{i.c.}} = L/\sqrt{N}$, where L is the surface size and N the cells number, which is the typical cell-cell distance. This length scale competes with r_A. For the physiologically interesting values of N ($N \geq 100$ for $L = 1$ mm), one has $r_{\text{i.c.}} < r_A$. Dynamical evolution, controlled by the action of the operator $\mathcal{L}$, can destroy this scale and rearrange matter in a network of typical length scale r_A.

The presence of a repulsive factor has the effect of screening high concentrations of activator in the cell proximity. In Fig. 3, the vector field $\mathcal{L}n$ is plotted for $\sigma = 0$ and 1. In the second case (perfect balance of repulsive and attractive ac-
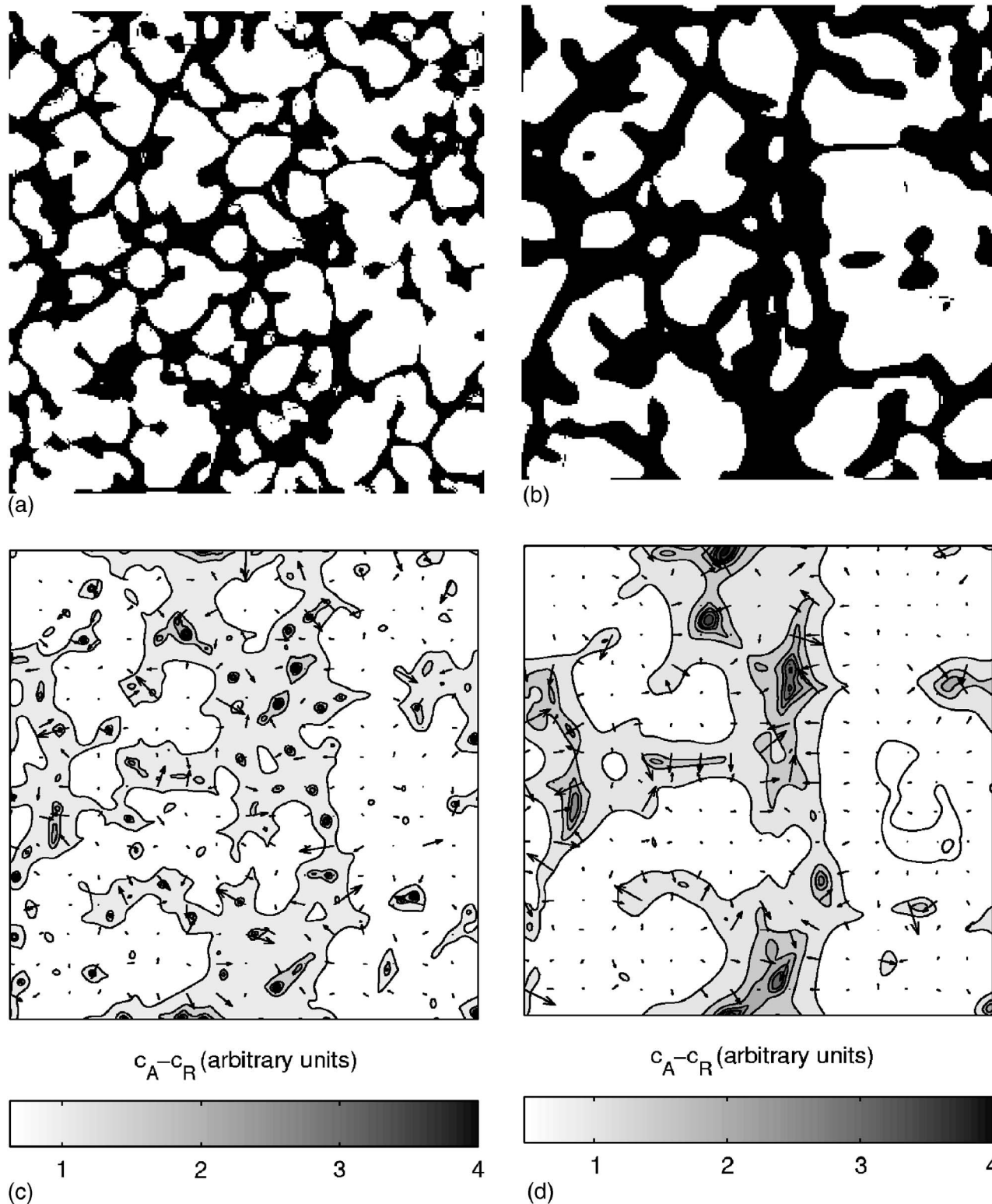
FIG. 4. Repulsive action results in larger reorganization of cellular matter, starting from the same initial conditions: (a) Final point of dynamical evolution in the presence of a purely attractive factor ($c_R=0$). (b) Final point of dynamical evolution in the presence of both attractive and repulsive factors ($\sigma=1$). Repulsive action results in a larger redistribution of cellular matter with respect to case (a). (c) Graph showing the concentration of attractive factor c_A for (a). Arrows indicate the gradient of c_A. (d) Graph showing the difference c_A-c_R between the concentration of attractive and repulsive factors for (b). Arrows indicate the gradient of c_A-c_R. Simulations were performed using $r_A=300$ μm, $r_R=150$ μm, and $\bar{n}=175$ cells/mm^2 on a square lattice of 256×256 nodes.
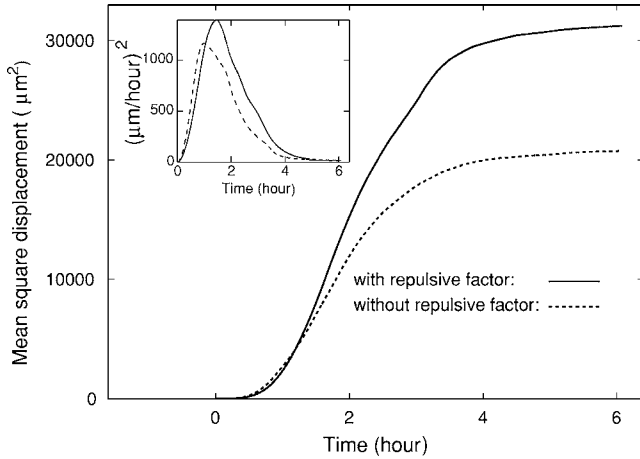
FIG. 5. Repulsive action results in larger reorganization of cellular matter. Main graph: time evolution of mean square displacement of cellular matter. Inset: time evolution of mean square velocities of cells. Solid line: dynamics in the presence of an attractive and a repulsive factor, as described in the text. Dashed line: dynamics in the presence of the sole attractive factor.

tion in the proximity of the cell), the effective attractive signal is more evenly distributed around the cell center. This real-space scenario corresponds to a faster decreasing asymptotic of the transfer function $\mathcal{L}_{\mathbf{k}}$, and is therefore expected to result in sharper control on the network dimensions. Repulsive factors agree, therefore, with the realization of a control on the structure dimensions by partially neutralizing autointeraction and depressing high wave numbers in
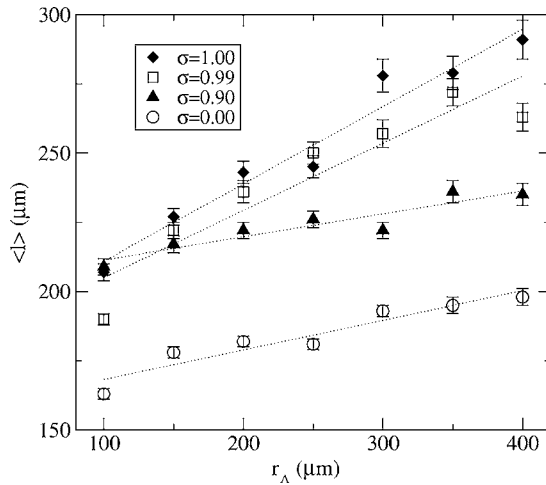

FIG. 6. Efficiency of the dynamical reorganization process for diffusion in a two-dimensional environment, observed on the dependency of the average chord length $\langle l \rangle$ on the interaction radius r_A, with varying relative contribution of attractive and repulsive factors. In the absence of repulsive factors ($\sigma=0$), an approximate linear dependence of $\langle l \rangle$ on r_A is observed. A larger reorganization efficiency is observed in the presence of repulsive factors ($\sigma \neq 0$). Maximal reorganization efficiency is obtained when the attractive and repulsive factors exactly compensate near the cells ($\sigma=1$). The results were obtained by 24 simulations of Eqs. (1) for each value of r_A letting $r_R=r_A/2$ and $\bar{n}=175$ cells/mm^2 using a square lattice of 256×256 nodes. Dotted lines are intended as guides for the eye.
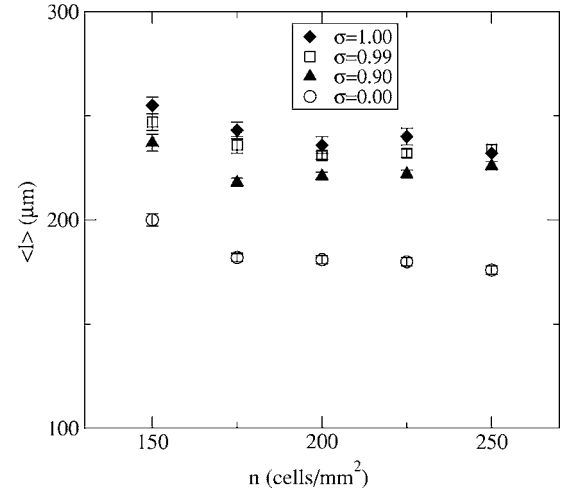

FIG. 7. Robustness of the dynamical reorganization process for diffusion in a two-dimensional environment, observed on the dependency of the average chord length $\langle l \rangle$ on the initial cell density $\bar{n}$, with varying relative contribution of attractive and repulsive factors, for fixed interaction radii $r_A=200$ μm, $r_R=100$ μm. The average chord length $\langle l \rangle$ is almost independent of the initial cell density $\bar{n}$ for each value of the relative contribution σ of attractive and repulsive factors, showing that control is robust and repulsive factors are not essential to confer robustness to the process of formation of a network geometry in a purely two-dimensional environment. The results were obtained by 24 simulations of Eqs. (1) for each value of the density $\bar{n}$ using a square lattice of 256×256 nodes.

the spectrum of $\mathcal{L}_{\mathbf{k}}$ (Fig. 2). This effect is maximum when $\sigma=1$, i.e., when repulsive and attractive factors perfectly balance in the cell proximity.

In order to describe in detail planar experiments of *in vitro* vasculogenesis, one should take into account the fact that while cell movement is confined on a two-dimensional surface (the Matrigel layer fixed to the bottom of a Petri dish), diffusion of soluble factors takes place on the overstanding liquid medium, i.e., in a three-dimensional half-space [31]. Denoting the Matrigel surface by $z=0$, the cell density by $n(x,y,z)=n(x,y)$ $\delta(z)$, and considering periodic boundary conditions, one obtains for the two-dimensional restriction of $\mathcal{L}_{\mathbf{k}}$

$$\mathcal{L}_{\mathbf{k}} = \left(i\frac{\pi\mu_A\alpha_A}{2D_A} \right)\left(\frac{\mathbf{k}}{\sqrt{r_A^{-2}+k^2}} - \sigma\frac{\mathbf{k}}{\sqrt{r_R^{-2}+k^2}} \right).$$

In this case, the difference between a purely attractive signal and a combined repulsive-attractive action is striking: as shown by the Bode plot for $\mathcal{L}_{\mathbf{k}}$ [Fig. 2(b)], for $\sigma=0$ (no repulsion) $\mathcal{L}_{\mathbf{k}}$ behaves as a high pass filter and does not exert any control on high wave numbers (short wavelengths). Instead, for $\sigma=1$ one has a high-order bandpass filter characterized by the asymptotic behavior $|\mathcal{L}_{\mathbf{k}}| \sim 1/k^2$. For intermediate values $\sigma \lesssim 1$, one observes a crossover for $k \sim 1/\sqrt{1-\sigma}$ to the $\sigma=0$ behavior.

This suggests that in dimensionally hybrid systems like the ones relevant to experimental assays, a control over
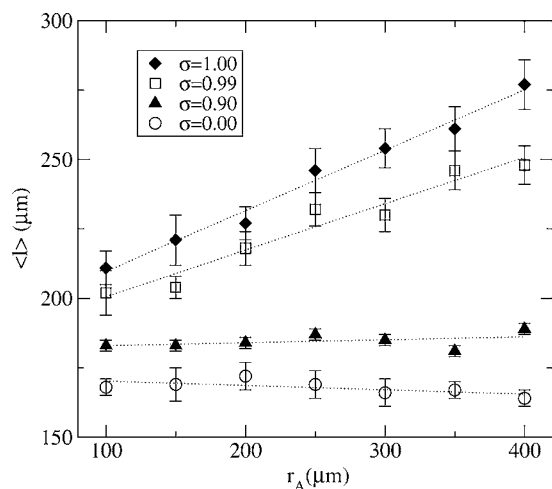
FIG. 8. Dynamical reorganization efficiency for diffusion in a three-dimensional environment, observed on the dependency of the average chord length $\langle l \rangle$ on the interaction radius r_A, for different relative contributions of attractive and repulsive factors. In the absence of repulsive factor ($\sigma = 0$), or when attractive and repulsive factors do not compensate near the cells ($\sigma < 1$), measured points lay on approximately flat lines, showing an absence of dynamical reorganization. The final state just inherits the scale $r_{\text{i.c.}}$ determined by the initial conditions. When attractive and repulsive factors compensate near the cells ($\sigma \simeq 1$), a clear dependence of $\langle l \rangle$ on r_A is observed, indicating efficient dynamical reorganization of the network. The results were obtained by 24 simulations of Eqs. (1) for each value of r_A letting $r_R = r_A/2$ and $\bar{n} = 175$ cells/mm^2 using a square lattice of 256×256 nodes. The three-dimensional diffusion equation (1c) was solved using a cubic lattice of $256 \times 256 \times 64$ nodes. Dotted lines are intended as guides for the eye.

length scales of observed structures can be obtained only if an attractive and a repulsive factor are present and $\sigma \simeq 1$.

IV. NUMERICAL RESULTS AND GEOMETRY OF THE NETWORK

In order to verify the validity of previous analytical arguments, we performed extensive numerical simulations of model (1) with two families of soluble molecules and values of the ratio σ varying between 0—no repulsive factors—and 1—perfect balance of attractive and repulsive factors in the cell proximity [32].

Simulations performed in the presence or absence of repulsive action show the qualitative fact that repulsive dynamics results in a larger reorganization of cellular matter (Fig. 4). A quantitative measure of this effect is the mean square displacement of cellular matter (Fig. 5). A better reorganization process requires that the distribution of cellular matter is reorganized on larger structures and, therefore, that cells travel over longer distances. Figure 5 shows that when both repulsion and attraction are present, the mean square displacement of cells is larger compared to the case in which only an attracting factor is present. This results in larger network structures and thicker chords (Fig. 4).

The degree of dynamical reorganization of network structures by attractive and repulsive factors is shown by the de-
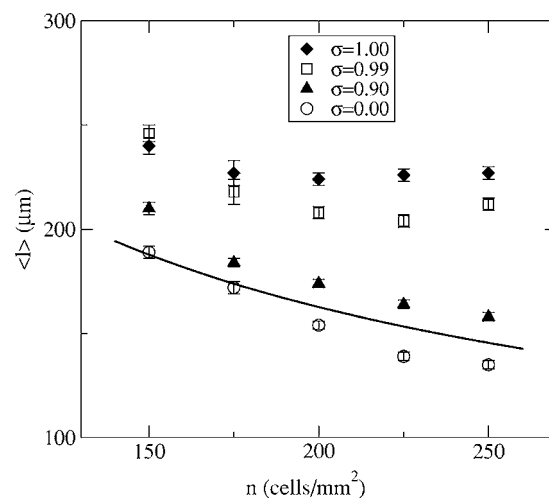

FIG. 9. Robustness of dynamical reorganization for diffusion in a three-dimensional environment, observed on the dependency of the average chord length $\langle l \rangle$ on the initial cell density $\bar{n}$ for varying relative contributions of attractive and repulsive factors, for fixed interaction radii $r_A = 200$ μm, $r_R = 100$ μm. When attractive and repulsive factors do not compensate in the cell proximity ($\sigma < 1$), the average chord length clearly depends on the initial cell density, showing the inefficiency of the control mechanism. A robust control is realized instead when repulsive and attractive factors compensate in the cell proximity ($\sigma \simeq 1$) since the average chord length is approximately independent of the initial cell density. Repulsive factors are therefore essential for robust control of the network geometry when diffusion takes place in a three-dimensional environment. As a reference, we plot the dependence $r_{\text{i.c.}} \propto 1/\sqrt{\bar{n}}$ of the scale length determined by the initial conditions on the initial density $\bar{n}$. The results were obtained by 24 simulations of Eqs. (1) for each value of the density $\bar{n}$ using a square lattice of 256×256 nodes. The three-dimensional diffusion equation (1) was solved using a cubic lattice of $256 \times 256 \times 64$ nodes.

pendence of the network statistical geometry on the interaction radii r_A, r_R. Efficient reorganization implies that geometrical properties of the network such as the average chord length are strictly regulated by the characteristic interaction radii r_A, r_R of the attractive and repulsive factors, and not by the characteristic length determined by the initial conditions. This length scale can in fact be destroyed by the dynamical reorganization process, which reorganizes cellular matter in a network of typical length r_A. Correspondingly, a robust control results in the statistical geometry not depending on the initial density $\bar{n}$. Such a robust control was observed in [7], where it was shown that the mean chord length is independent of the density $\bar{n}$ over a range of values extending from 100 to 250 cells/mm^2.

To investigate how the interaction radii r_A, r_R of the attractive and repulsive factors control the geometrical properties of the observed vascular structures, we have measured the chord length distribution resulting from a large number of random realizations of the initial conditions, varying r_A for fixed r_A/r_R [33,34] (the chord length distribution has been measured by the algorithm described in the Appendix). To study the robustness of the geometrical control, we have also studied how the average chord length varies changing the average density $\bar{n}$ for fixed r_A, r_R.
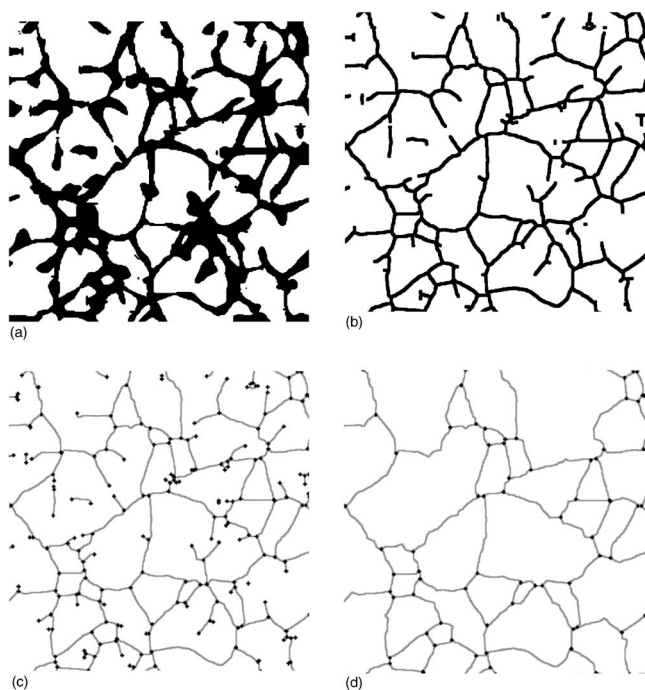
FIG. 10. (a) Two-level image obtained through numerical simulation, for diffusion in a three-dimensional environment with r_A =100 μm, r_R=50 μm, and σ=1. (b) Skeleton obtained by applying the proposed thinning procedure. (c) Representation as a formal graph. (d) Formal graph after pruning step.

For diffusion in a two-dimensional environment, results are shown in Figs. 6 and 7. Figure 6 shows an approximate linear dependence of the network geometry on the interaction radius r_A in the absence of repulsive factors (σ=0), as reported in [7]. The presence of repulsive factors ($\sigma \simeq 1$) results in larger structures and in more efficient control on the length scale, i.e., in an approximately linear dependence of the average chord length $\langle l \rangle$ on r_A with a slope that grows with σ. In the presence of repulsive factors, then, cellular matter is more efficiently reorganized and the scale $r_{i.c.}$ introduced by the initial conditions is dynamically substituted by the interaction radius r_A. Figure 7 shows that $\langle l \rangle$ is almost independent of $\bar{n}$ for each σ. This implies that for diffusion in a two-dimensional environment, control is always robust even without the action of repulsive factors.

We then simulated diffusion in three-dimensional half-space with reflecting boundary conditions, coupled to two-dimensional cell transport on the frontier of the half-space. Results are shown in Figs. 8 and 9. Figure 8 shows that the graphs of the average chord length $\langle l \rangle$ as a function of the interaction radius r_A are flat when attractive and repulsive factors do not balance perfectly in the cell proximity, $\sigma < 1$, indicating that the network geometry does not depend on the interaction radius r_A and that there is no dynamical reorganization of the structures. In the case of perfect balance between attractive and repulsive factors in the cell proximity ($\sigma \simeq 1$), a clear dependence of the average chord length $\langle l \rangle$ on r_A is instead observed, showing the efficiency of dynamical reorganization.

Figure 9 indicates that for diffusion in a three-dimensional environment, robust reorganization of the network geometry

is realized only when attractive and repulsive factors balance in the cells proximity. In this case ($\sigma \simeq 1$), the structure size is determined by r_A and control on the typical length scale is robust, since $\langle l \rangle$ is almost independent of the initial cells density.

In standard experimental conditions [7,18] soluble factors actually diffuse in 3D in the fluid medium, while cell movement is confined to the 2D Matrigel surface, corresponding to the dimensionally hybrid situation described by our simulations. In these conditions, it has been experimentally checked that the average chord length of observed networks does not depend on the initial cell density [7,15], i.e., on $r_{i.c.}$. Comparison with the results of the simulations (Fig. 9), where dependence on r_A is actually observed only when the attractive action is balanced by repulsion on scales of the order of the cell size, suggests that repulsive factors are actually playing a role in determining the size of patterns in experimental vasculogenesis.

V. CONCLUSIONS

We presented a model for *in vitro* vascularization experiments, which generalizes the model proposed in Ref. [6] in order to take into account the presence of more families of soluble chemotacting factors, and in particular the presence of repulsive factors. The model allows us to discuss the question of geometrical robustness in the process of vascular network formation, which is physiologically relevant, since the size of capillaries is strictly related to their functionality. Recent experiments [4] have shown that the role of repulsive factors is essential to ensure the necessary degree of plasticity of vascular networks. They allow a graded control of cellular migration rate and redirecting during migration.

Our results show that the presence of repulsive factors allows a better reorganization process and a better control on the size of the resulting patterns. From a mathematical point of view, the main geometrical properties of the observed networks are encoded in the integral operator which solves the equation of diffusion for the chemical factors. In particular geometries, for example in dimensionally hybrid situations similar to the ones realized in *in vitro* experiments, reorganization of the initial configuration and robust control on the final configuration size can be ensured only in the presence of at least an attractive and a repulsive factor, whose actions balance in the cell proximity.

We expect that this theoretical prediction will be the subject of future experimental studies, focusing on the question of how control on the geometrical properties of vascular networks is realized and which role repulsive factors play in the morphogenetic process.

Another area where our model could be tested is the study of vascularization in living beings [9]. It is known that various VEGF-A isoforms with different diffusion constants (providing different length scales) exist. Removing the less diffusible forms of VEGF-A by gene targeting leads to the formation of vascular structures characterized by different length scales [9], as suggested by our model. This could be another step to a more quantitative understanding of the molecular mechanisms of vascularization.
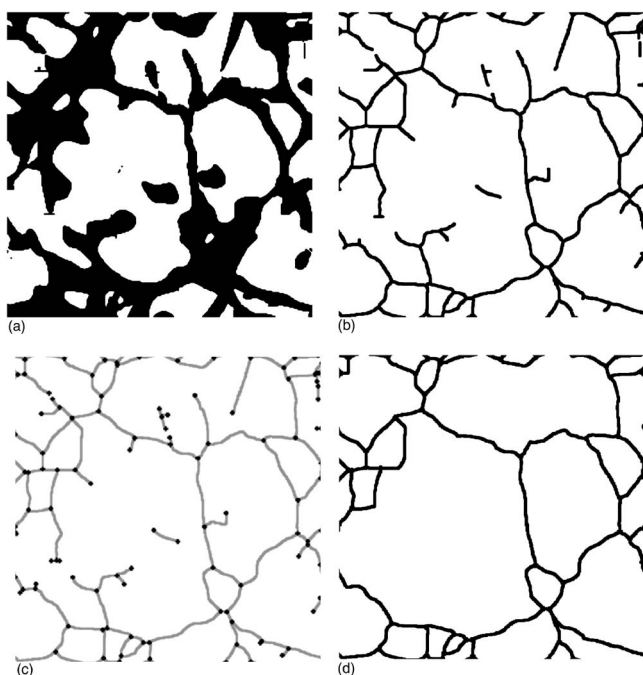
FIG. 11. (a) Two-level image obtained through numerical simulation, for diffusion in a three-dimensional environment with r_A =400 μm, r_R=200 μm, and σ=1. (b) Skeleton obtained by applying the proposed thinning procedure. (c) Representation as a formal graph. (d) Formal graph after pruning step.
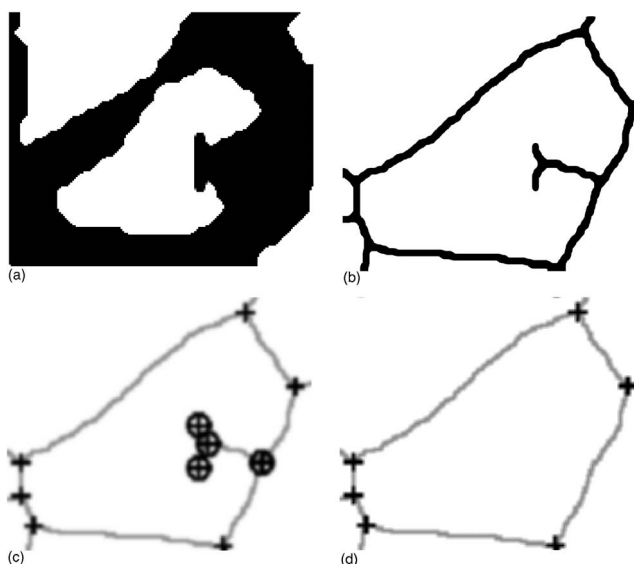

FIG. 12. Details of the pruning procedure. (a) Particular of a two-level image obtained through simulation. (b) Skeleton: line fuzz artifacts originated by the thinning algorithm are clearly visible. (c) Graph-based representation reconstructed from the adjacency list before pruning (circles indicate vertices that have to be removed from the adjacency list together with leaving edges). (d) Graph-based representation after removal of irregular vertices and edges (canceled edges are replaced by new edges being the aggregation of constituting edges).

Different theoretical models for *in vitro* vascularization have been proposed [35–37], focusing on cellular network reorganization driven by cellular traction [38]. These models were initially motivated by experiments performed with bovine aortic endothelial cells (BAECs) [35,38]. Both our model and this class of models are mathematical idealizations of reality, obtained in different physical/biological limits. Our model is obtained in the limit in which mechanic effects are negligible and cell motion is mainly directed, while models of Refs. [35–37] are obtained in the limit in which mechanic effects are dominant. Both classes of models reproduce well the vascular patterning and different experimental observations and therefore neither of them seems currently complete. We believe, however, that the physical/ biological limits in which the models are obtained may be realizable under different laboratory conditions. In the assays described in Ref. [7], directed, amoeboid cell motion is clearly observed [39], autocrine production of VEGF-A is also directly observed, and stress-induced deformation of the matrix substrate does not appear in the first hours of observation, but only toward the end of the vasculogenic process, which, as is explicitly stated in Ref. [7], is not described by our model. Instead, in the assays described in Ref. [38] and modeled in Ref. [35], stress-induced deformations of the gel matrix are observed from the very beginning. We argue that the difference between the two experiments lies both in the different cell density and in the use of different endothelial cell (EC) populations in the two cases: human ECs from umbilical vein (HUVEC) and adrenal cortex versus bovine ECs from aorta (BAEC). In any case, the predominance of amoeboid directed motion in our models (HUVEC and human adrenal cortex ECs) and of motion along stress-induced deformations (mesenchymal migration) in Vernon's experiments with BAEC is clear from the photographs of the experiments. Ameboid and mesenchymal migration can be considered as different programs that an individual cell is able to execute (for a distinction between amoeboid and mesenchymal migration, see, for example, Ref. [40]). We would also like to stress that network formation would be observed in our model even without chemotaxis [29,30]. What chemotaxis adds to the picture is a plausible means of controlling the network characteristic scale. This mechanism could in principle be quite sophisticated, as explained in the present paper. Our group [7] and others [8,16–19] have shown the presence and the possible function of autocrine VEGF-A in ECs during vascular network formation both *in vitro* and *in vivo*. We hope that our present work encourages a more complete and direct analysis of the function and the dynamics of chemoattractive and chemorepulsive molecules during *in vitro* vasculogenesis.

Finally, we observe that cell-centered models [41,42] derived from the model of Ref. [6] have recently confirmed the main results of Refs. [6,7]. These models compared with continuous models have the advantage that different physicochemical properties can be assigned to each cell and their effects on the vascular pattern can be easily studied. These individual cell models should be easily extended to reproduce the structure of the generalized model presented in this paper.

ACKNOWLEDGMENTS

APPENDIX: IMAGE ANALYSIS

In this appendix, we present an unsupervised analysis system enabling fully automated processing of two-level images obtained through numerical simulations. The overall methodology can be broken up into several consecutive steps that lead to the generation of a graph-based representation of the blood vessel network, which allows us to evaluate effectively and accurately network-related parameters.

A skeletonization procedure is first applied on simulation images [see Fig. 10(a) and 11(a), which are representatives of simulations performed with $r_A = 100$ and 400 μm, respectively] in order to extract a thinned image conveying essential structural information, thus simplifying the measurement task. Skeletonization is defined as the act of identifying those pixels belonging to an object that are essential for communicating the object's shape, preserving its topological properties [43]. The skeletonization step has been deployed using a thinning-based approach. The majority of thinning algorithms are based on a repeated stripping away of layers of pixels until no more layers can be removed. There is a set of rules defining which pixels may be removed, and frequently some sort of template-matching scheme is used to implement these rules. In this work, we selected the well-established Zhang-Suen implementation [44], which is capable of producing a sufficiently accurate skeleton. Nevertheless, there exists some problems with thinning algorithms that show up as artifacts in the skeleton. The first of these is called *necking*, in which a narrow point at the intersection of two lines is stretched into a small line segment. Also, *tails* can be created where none exist because of excess thinning where two lines meet at an acute angle. Finally, *hairs* or *line fuzzes* (the creation of extra line segments joining a real skeleton segment) frequently appear. To minimize these thinning artifacts, we adopted the preprocessing and the postprocessing stages proposed by Stentiford and Holt [45,46]. Figures 10(b) and 11(b) show the skeleton images resulting from the application of the aforementioned skeletonization procedure to the simulation images in Figs. 10(a) and 11(a), respectively.

A formal graph-based description of the vessel network is then extracted from the skeletonized image by using a novel image-based implementation of the breadth-first search algorithm [47]. In this way, an adjacency list containing all the vertices, together with pixels belonging to the edges leaving and entering each vertex, is generated. The availability of such a representation constitutes the basis for accurate network's parameters measurement. Figures 10(c) and 11(c) show the graphical representation of the formal graphs extracted from the skeleton images in Figs. 10(b) and 11(b), respectively. Most of the artifacts produced by the thinning step are removed by introducing preprocessing and postprocessing steps in the skeletonization procedure. Nevertheless, several line fuzzes that do not actually represent any structural feature in the considered simulation image are still present in the skeleton [see Figs. 12(a) and 12(b)]. A pruning operation is therefore performed on the skeleton image in order to remove these artifacts [Fig. 12(c)] and a refined image based on information collected during graph extraction is reconstructed [Fig. 12(d)]. Figures 10(d) and 11(d) show the graphical representation of the formal graphs in Figs. 10(c) and 11(c) after pruning, respectively. Finally, a minimum closed-circuits discovery procedure is applied on the graph in order to identify those edges depicting a closed structure within the image. The adjacency list maintaining the ordered list of skeleton pixels constituting each edge of the undirected graph representing the vessel network together with the closed-circuits list have then been used to measure capillary chords length.

[1] N. Barkai and S. Leibler, Nature (London) **387**, 913 (1997).

[2] M. E. Csete and J. C. Doyle, Science **295**, 1664 (2002).

[3] A. Turing, Philos. Trans. R. Soc. London, Ser. B **237**, 37 (1952).

[4] G. Serini *et al.*, Nature (London) **424**, 391 (2003).

[5] P. Carmeliet, Nat. Med. **6**, 389 (2000).

[6] A. Gamba, D. Ambrosi, A. Coniglio, A. de Candia, S. Di Talia, E. Giraudo, G. Serini, L. Preziosi, and F. Bussolino, Phys. Rev. Lett. **90**, 118101 (2003).

[7] G. Serini, D. Ambrosi, E. Giraudo, A. Gamba, L. Preziosi, and F. Bussolino, EMBO J., **22**, 1771 (2003).

[8] N. Tang, L. Wang, J. Esko, F. J. Giordano, Y. Huang, HP. Gerber, N. Ferrara, and R. S. Johnson, Cancer Cells **6**, 485 (2004).

[9] C. Ruhrberg, H. Gerhardt, M. Golding, R. Watson, S. Ioannidou, H. Fujisawa, C. Betsholtz, and D. T. Shima, Genes Dev. **16**, 2684 (2002).

[10] A. C. Guyton and J. E. Hall, *Textbook of Medical Physiology*, 10th ed. (W.B. Saunders, St. Louis, 2000).

[11] R. J. Tomanek, *Assembly of the Vasculature and its Regulation* (Birkhauser, Boston, 2002).

[12] R. S. Cotran, V. Kumar, T. Collins, S. L. Robbins, and B. Schmitt, *Robbins Pathologic Basis of Disease*, 6th ed. (Saunders, Philadelphia, 1999).

[13] Y. Kubota, H. K. Kleinman, G. R. Martin, and T. J. Lawley, J. Cell Biol. **107**, 1589 (1988).

[14] D. S. Grant, K. Tashiro, B. Segui-Real, Y. Yamada, G. R. Martin, and H. K. Kleinman, Cell **58**, 933 (1989).

[15] A. Coniglio, A. de Candia, S. Di Talia, and A. Gamba, Phys. Rev. E **69**, 051910 (2004).

[16] G. Seghezzi, S. Patel, C. J. Ren, A. Gualandris, G. Pintucci, E. S. Robbins, R. L. Shapiro, A. C. Galloway, D. B. Rifkin, and P. J. Mignatti, J. Cell Biol. **141**, 1659 (1998).

[17] H. Yonekura, S. Sakurai, X. Liu, H. Migita, H. Wang, S. Yamagishi, M. Nomura, M. J. Abedin, H. Unoki, Y. Yamamoto, and H. Yamamoto, J. Biol. Chem. **274**, 35172 (1999).

[18] D. Wang, R. E. Lehman, D. B. Donner, M. R. Matli, R. S. Warren, and M. L. Welton, Am. J. Physiol. Gastrointest. Liver

Physiol. **282**, G1088 (2002).

[19] D. Virgintino, M. Errede, D. Robertson, F. Girolamo, A. Masciandaro, and M. Bertossi, Histochem. Cell Biol. **119**, 227 (2003).

[20] E. Tischer *et al.*, J. Biol. Chem. **266**, 11947 (1991).

[21] K. A. Houck *et al.*, J. Biol. Chem. **267**, 26031 (1992); J. E. Park, Mol. Biol. Cell **4**, 1317 (1993).

[22] J. Grunstein, J. J. Masbad, R. Hickey, F. Giordano, and R. S. Johnson, Mol. Cell. Biol. **20**, 7282 (2000).

[23] F. Filbet, P. Laurencot, and B. J. Perthame, J. Math. Biol. **50**, 189 (2005).

[24] Different functional forms for $f(n)$ have been tested yielding very similar results. The simulations have been performed with $f(n)=0.5+\arctan[a*(n-n_0)]/\pi$, $a=100$, $n_0=8$.

[25] The finite velocity of diffusion renormalizes these scales by factors of order 1. Let us consider, for instance, the evolution of the chemical concentration $c(x,t)$ in one spatial dimension and in the case of the simple source term $n(x,t)=f(x-vt)+f(x+vt)$, representing two cells that move away from each other with velocity v. Equation (1c) becomes in Fourier space $(-i\omega+Dk^2+\tau^{-1})c_{k,\omega}=f(k)[\delta(\omega-kv)+\delta(\omega+kv)]$. Solving this equation and inverting the FT, the dynamics is seen to renormalize the characteristic length scales r_k. The effect depends on the characteristic velocities of the system, and becomes relevant when the system's typical velocity v becomes $v \gg \sqrt{D/\tau}$. The experiments show that the characteristic cell velocity is $v \sim \sqrt{D/\tau}$, so the renormalization factor is of order 1 and the fast diffusion approximation is qualitatively correct.

[26] To maintain the substantially attractive mechanism of cell communication, we shall assume that $\sigma \leq 1$.

[27] A. Pluen, P. A. Netti, R. K. Jain, and D. A. Berk, Biophys. J. **77**, 542 (1999).

[28] J. Burgers, *The Non Linear Diffusion Equation* (D. Reidel Publ. Co., Dordrecht, 1974).

[29] S. F. Shandarin and Ya. B. Zeldovich, Rev. Mod. Phys. **61**, 185 (1989).

[30] M. Vergassola, B. Dubrulle, U. Frisch, and A. Noullez, Astron. Astrophys. **289**, 325 (1994).

[31] Since the mass of soluble factors is ~ 200 kDa and experiments are performed at $T=37\,^{\circ}$C, weight becomes relevant at a height $h \sim 1$ m. Petri dishes are filled with ~ 0.5 cm of liquid and we can assume that soluble molecules are freely diffusing in 3D over the 4 mm^2 observed surface.

[32] The numerical simulations were performed on square boxes of size $L=2$ mm with periodic boundary conditions, using a finite volume method. We used the experimental values for D and τ, while the unknown parameters μ, α were set to 1 (which amounts to appropriate rescaling of time and the concentration field c). The initial conditions were given by throwing the same number of cells as in the biological experiments in random positions inside the box, with zero velocities and zero concentration of the soluble factor, with a single cell given initially by a Gaussian bump of width $\sigma=30$ μm and unitary weight in the integrated cell density field n. Starting from these conditions, Eqs. (1) were numerically integrated. The simulation was stopped when the vascular network was formed, or a stationary state was reached. In the figures, black areas represent regions filled with cells, that is, regions where the density exceeds a given threshold; white areas represent the underlying substrate. The threshold was chosen to coincide with the close-packing density $\sim 1/(2\pi\sigma^2)$.

[33] F. Lamberti, A. Gamba, and B. Montrucchio, Journal of WSCG **12**, 237 (2004); also available at: http://wscg.zcu.cz/wscg2004/Papers_2004_Full/M37.pdf

[34] F. Lamberti and B. Montrucchio, *Proceedings of the IEEE International Symposium on Biomedical Imaging: From Nano to Macro* (IEEE, Piscataway, NJ, 2004), pp. 129–132.

[35] D. Manoussaki, S. R. Lubkin, R. B. Vernon, and J. D. Murray, Acta Biotheor. **44**, 271 (1996).

[36] J. D. Murray, Comptes Rendus de la Academie des Sciences de Paris (Biologies) **326**, 230 (2003).

[37] P. Namy, J. Ohayon, and P. J. Tracqui, J. Theor. Biol. **227**, 103 (2004).

[38] R. B. Vernon, J. C. Angello, M. L. Iruela-Arispe, T. F. Lane, and E. H. Sage, Lab. Invest. **66**, 536 (1992).

[39] See the supplementary on-line movie of Ref. [7], http://www.nature.com/emboj/journal/v22/n8/extref/7595085s2.mov.

[40] P. Friedl, Curr. Opin. Cell Biol. **16**, 14 (2004).

[41] R. M. H. Merks, S. A. Newman, and J. A. Glazier, Lect. Notes Comput. Sci. **3305**, 425 (2004).

[42] R. M. H. Merks and J. A. Glazier, q-bio.TO/0505033.

[43] The precise definition of the skeleton of a region R with border B is the following: for each p in R, find its closest neighbor in B. If p has more than one such closest neighbor, then p belongs to the skeleton of R.

[44] R. C. Gonzales and R. E. Woods, *Digital Image Processing* (Addison-Wesley, Reading MA, 1993).

[45] C. M. Holt *et al.*, Commun. ACM **2**, 156 (1987).

[46] F. W. M. Stentiford *et al.*, IEEE Trans. Syst. Man Cybern., **1**, 81 (1983).

[47] E. F. Moore, *The Shortest Path Through a Maze*, in Proceedings of the International Symposium on the Theory of Switching Conference (Harvard University Press, MA, 1959), pp. 285–292.